ARMY RESEARCH LABORATORY

High-Speed Photographic Study of Wave Propagation and Impact Damage in Transparent Aluminum Oxynitride (AlON)

by Elmar Straßburger

ARL-CR-579 **September 2006**

prepared by

Fraunhofer-Gesellschaft zur Förderung der angewandten Forschung e.V.
Hansastraße 27c, D-80686
München, Germany

for

U.S. Army Research Laboratory
Aberdeen Proving Ground, MD 21005

under contract

N62558-04-P-6031

NOTICES

Disclaimers

The findings in this report are not to be construed as an official Department of the Army position unless so designated by other authorized documents.

Citation of manufacturer's or trade names does not constitute an official endorsement or approval of the use thereof.

Destroy this report when it is no longer needed. Do not return it to the originator.

Army Research Laboratory
Aberdeen Proving Ground, MD 21005-5069

ARL-CR-579 **September 2006**

High-Speed Photographic Study of Wave Propagation and Impact Damage in Transparent Aluminum Oxynitride (AlON)

Elmar Straßburger

prepared by

Fraunhofer-Gesellschaft zur Förderung der angewandten Forschung e.V.
Hansastraße 27c, D-80686
München, Germany

for

U.S. Army Research Laboratory
Aberdeen Proving Ground, MD 21005

under contract

N62558-04-P-6031

REPORT DOCUMENTATION PAGE

Form Approved
OMB No. 0704-0188

1. REPORT DATE *(DD-MM-YYYY)*	2. REPORT TYPE	3. DATES COVERED (From - To)
September 2006	Final	July 2004–July 2005

4. TITLE AND SUBTITLE
High-Speed Photographic Study of Wave Propagation and Impact Damage in Transparent Aluminum Oxynitride (AlON)

5a. CONTRACT NUMBER
N62558-04-P-6031

5b. GRANT NUMBER

5c. PROGRAM ELEMENT NUMBER

6. AUTHOR(S)
Elmar Straßburger

5d. PROJECT NUMBER
487581M071

5e. TASK NUMBER

5f. WORK UNIT NUMBER

7. PERFORMING ORGANIZATION NAME(S) AND ADDRESS(ES)
Fraunhofer-Gesellschaft e.V.
Hansastrassee 27c
D-80686 München
Germany

Fraunhofer-Institut für Kurzzeitdynamik
Ernst-Mach-Institut
Am Klingelberg 1
D-79588 Efringen-Kirchen
Germany

8. PERFORMING ORGANIZATION REPORT NUMBER

9. SPONSORING/MONITORING AGENCY NAME(S) AND ADDRESS(ES)
U.S. Army Research Laboratory
ATTN: AMSRD-ARL-WM
Aberdeen Proving Ground, MD 21005-5069

10. SPONSOR/MONITOR'S ACRONYM(S)

11. SPONSOR/MONITOR'S REPORT NUMBER(S)
ARL-CR-579

12. DISTRIBUTION/AVAILABILITY STATEMENT
Approved for public release; distribution is unlimited.

13. SUPPLEMENTARY NOTES

14. ABSTRACT

Fused silica and AlON specimens were tested by means of a modified edge-on impact technique. The specimens were placed between crossed polarizers, and the photo-elastic effect was utilized to visualize the stress waves. Pairs of impact tests at approximately equivalent velocities were carried out in transmitted plane (shadowgraphs, visualization of damage) and crossed polarized light (visualization of wave propagation). The experiments provided direct evidence of ceramic damage by nucleation and growth of fracture initiated by the stress waves, ahead of the coherent fracture front growing from the impacted edge. A comparison of the results in a reflected light set-up and the shadowgraphs indicated fracture nucleation in the interior of the ceramic. The experimental results provide a data basis for a deeper analysis of the damage mechanisms by means of numerical simulation. The work was supported by Dr. Douglas Templeton, U.S. Army Tank-Automotive Research, Development and Engineering Center, Warren, MI.

15. SUBJECT TERMS
high-speed photography, wave propagation, damage propagation, AION

16. SECURITY CLASSIFICATION OF:			17. LIMITATION OF ABSTRACT	18. NUMBER OF PAGES	19a. NAME OF RESPONSIBLE PERSON
a. REPORT	b. ABSTRACT	c. THIS PAGE			James McCauley
UNCLASSIFIED	UNCLASSIFIED	UNCLASSIFIED	UL	40	19b. TELEPHONE NUMBER (*Include area code*) 410-306-0711

Standard Form 298 (Rev. 8/98)
Prescribed by ANSI Std. Z39.18

Contents

List of Figures

List of Tables

Preface

The research reported in this report has been made possible through the support and sponsorship of the U.S. Government through its European Research Office of the U.S. Army. This report is intended only for the internal management use of the contractor and the U.S. Government. Research was carried out in collaboration with Dr. Parimal Patel and Dr. James W. McCauley of the U.S. Army Research Laboratory and Dr. Douglas Templeton of the U.S. Army Tank-Automotive Research, Development and Engineering Center.

1. Introduction

When a high-speed projectile hits a brittle material like glass or ceramic, severe fragmentation can be observed, preceding the penetration of the projectile. Several types of glass (*1*, *2*) ceramic (*3*), and a glass-ceramic (*4*) have already been studied at Ernst-Mach-Institut (EMI) by means of the edge-on impact test.

Fused silica and aluminum oxynitride (AlON) are materials being considered for a variety of transparent armor, sensor window, and radome applications. AlON is a polycrystalline ceramic that fulfills the requirements of transparency and requisite mechanical properties for transparent armor against armor-piercing ammunition (*5*). AlON has a cubic crystal structure (Fd3m) that can be processed to transparency in a polycrystalline microstructure. It differs from glasses which do not have any periodic crystalline order, but is akin to polycrystalline opaque ceramics such as aluminum oxide.

In the current study, two different optical configurations were employed. A regular transmitted light shadowgraph set-up was used to observe wave and damage propagation and a modified configuration, where the specimens were placed between crossed polarizers and the photo-elastic effect was utilized to visualize the stress waves. Pairs of impact tests at approximately equivalent velocities were carried out in transmitted plane (shadowgraphs) and crossed polarized light. AlON and fused silica specimens were impacted using solid cylinder steel projectiles with velocities ranging from 270 to 925 m/s. The nucleation of crack centers was observed ahead of the apparent fracture front, growing from the impacted edge of the specimens. A comparison of the shadowgraphs to photographs recorded in a reflected light configuration with a coated AlON specimen at the same impact conditions indicated fracture nucleation in the interior of the ceramic.

2. Statement of Work

2.1 Results With Fused Silica

The optical configurations and the experimental results have been described and discussed in detail in the first and second interim reports (*6*, *7*) and in a publication at the 22nd International Symposium on Ballistics (*8*). Therefore, only a short summary and discussion of the results is given here.

The tests were performed as one single shot at 125 m/s and three pairs of shots at nominal impact velocities of 150, 250, and 350 m/s. With each pair of shots one test was conducted in the regular shadowgraph configuration and the other test with additional crossed polarizers. The test matrix is given in table 1. The last two columns list the time intervals between the photographs. In each test, 20 photographs were recorded.

Table 1. Tests with fused silica.

Test No.	**Impact Vel. (m/s)**	**Set-up**	**Time Intervals**	
14885	125	No polarizers	1-16: 1 µs	16-20: 2 µs
14880	155	No polarizers	1-16: 1 µs	16-20: 2 µs
14881	≈150	Crossed polarizers	1-16: 1 µs	16-20: 2 µs
14891	≈260	No polarizers	1-20: 1 µs	—
14893	262	Crossed polarizers	1-20: 1 µs	—
14877	350	Crossed polarizers	1-13: 1 µs	13-20: 2 µs
14878	348	No polarizers	1-13: 1 µs	13-20: 2 µs

The velocities specified with test nos. 14881 and 14891 were estimated on the basis of the thickness of the aluminium diaphragm used in the gas gun. Due to the high reproducibility observed it can be assumed that the impact velocity in those tests was within a range of ±10 m/s around the impact velocity of the other test with the same diaphragm thickness.

Figure 1 shows eight shadowgraphs and the corresponding crossed polarizers photographs of two tests conducted at 350 m/s. Note that damage appears dark on the shadowgraphs and the zones with stress birefringence are exhibited as bright zones in the crossed polarizers photographs. The shadowgraphs and crossed polarizers photographs are aligned one below the other, allowing for a direct comparison. The time of each pair of photographs is denoted in the crossed polarizers photographs. The moment of impact (t = 0 µs) was determined by means of a short circuit between two trigger foils at the impact edge of the specimens, generated by the projectile.

On the shadowgraphs it can be seen that damage starts first where the edge of the projectile impacts the specimen. Triangularly shaped damage zones spread towards the upper and lower edge of the specimen. The photographs also show the rapid growth of separated, damage zones ahead of the projectile, seemingly due to crack nucleation and growth apparently created by the stress wave interaction with pre-existing processing defects or structural inhomogenieties in the fused silica. The stress waves itself exhibits a relatively plane front in the centre and a curved shape outwards.

Unlike the shadowgraphs, in the crossed polarizers pictures an approximately semicircular wave front can be recognized, which is further advanced compared to the front visible in the shadowgraphs at the same time. However, the stress wave is not as clearly defined (especially in the center) as the actual damage front in the shadowgraphs. The vertical lines in some pairs of photographs indicate the position of the wave front in the crossed polarizers view.

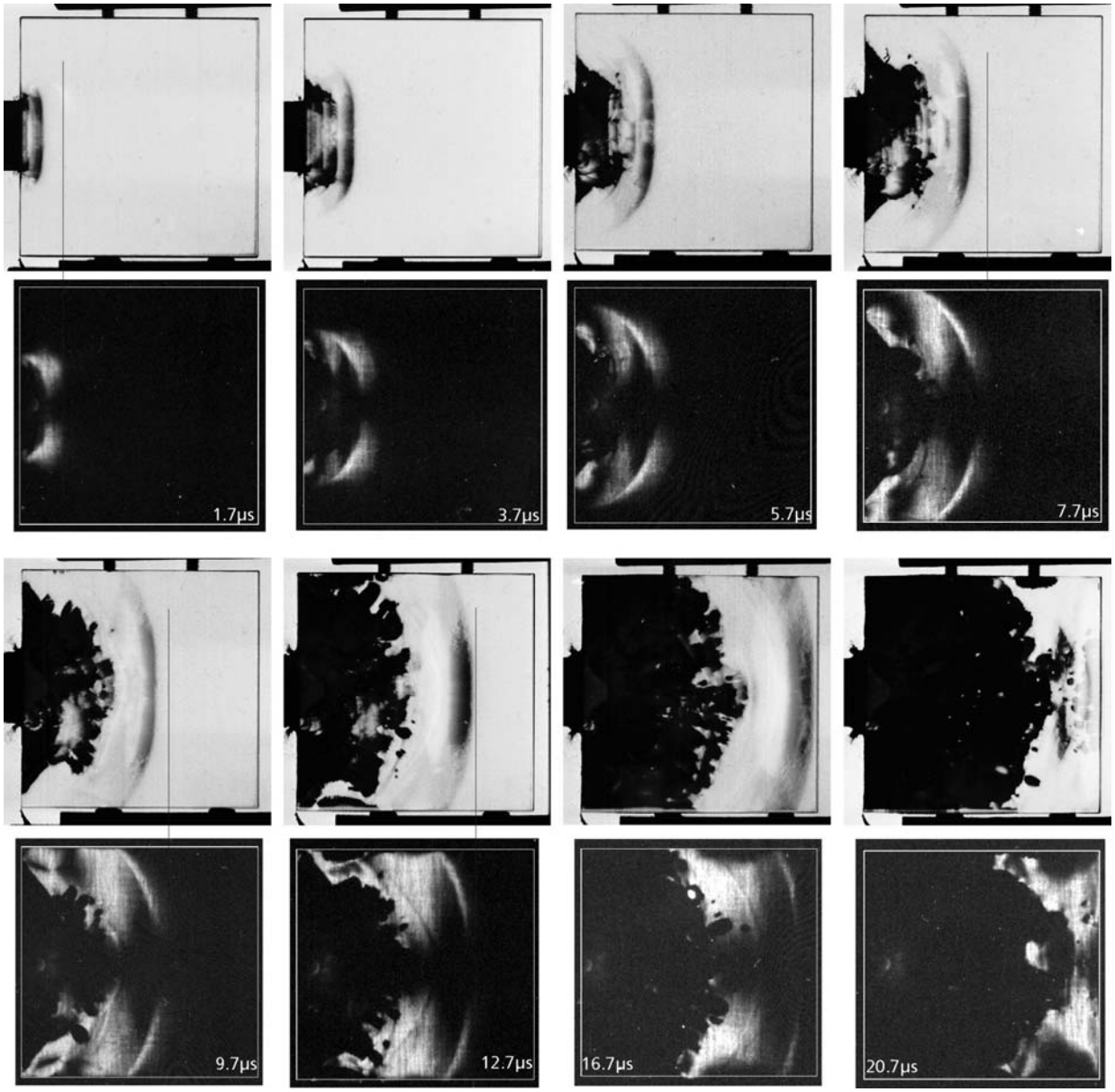

Figure 1. Test no. 14877-78: Selection of eight shadowgraphs and corresponding crossed polarizers photographs from impact on fused silica at 350 m/s.

The photographs taken with the two different recording techniques reveal different processes. In the crossed polarizers arrangement, those zones of the specimen are visible, where the stresses are high enough to cause birefringence, so that enough light passes through in order to expose the film. Basically, in the crossed polarized light configuration, the stress field is visualized because of stress induced birefringence—i.e., the photoelastic effect. In the regular shadowgraph arrangement, those zones of the specimen appear dark, where the material is either damaged or fractured and therefore blocking light transmission or where the light is absorbed more strongly due to a pressure induced change in refractive index.

The quantitative results for wave and damage/fracture velocities are presented in table 2. Considering the wave front velocities, determined with both optical set-ups, the same observation was made at all impact velocities: the wave front was further advanced in the crossed polarizers view (see figure 1), but the wave velocity was lower compared to the waves observed in the shadowgraphs (see table 2).

Table 2. Compilation of measured wave, crack, and damage velocities in fused silica.

Impact Velocity v_P	**Set-up**	**m/s**	**150**	**260**	**350**
Long. wave speed	Shadowgraphs	m/s	5975	6076	5823
Long. wave speed	Crossed polarizers	m/s	5814	5796	5491
Trans. wave speed	Shadowgraphs	m/s	—	3500	3670
Crack velocity	Shadowgraphs	m/s	2234	2149	2120
Damage velocity	Shadowgraphs	m/s	5641	5728	5121

The correct interpretation of the results requires an understanding of the dependence of the deflection of light on the loading of the specimens. In order to distinguish between light deflections caused by surface deformation and deflections caused by changes of the refractive index, a reflection Schlieren set-up was devised at EMI by H. Vollkommer (*9*) in which glass plates were loaded at one edge by a wire explosion. The upper half of the glass specimen was coated with a reflective layer at the front surface and the lower half was similarly coated at the back surface. The tests demonstrated that, in the zone of the longitudinal waves, surface deformation is irrelevant, while the refractive index changes dominate, whereas behind the transversal wave front, light deflection through surface deformation is the dominant effect. In a shadowgraph image the light intensity depends on the second spatial derivative $\partial^2 n/\partial x^2$ of the refractive index (*10*). When the photo-elastic behavior of a material is known the amplitudes of the pressure pulses can be determined. Beinert (*11*) developed a method to calibrate a Schlieren set-up and measured the amplitude and shape of pressure pulses in glass plates generated by wire explosions at one edge.

In the present study neither the shapes of the pressure pulses are known, nor whether the pulse shapes change during propagation in the edge-on impacted plates. However, the amplitude and shape of pressure pulses determine where the change in density, and therefore in the refractive index, is strong enough to cause a deflection of light that can be detected with the optical set-up used. The sequence of events along the pressure pulse/wave may be assumed to be as follows: rising pressure induces a density increase causing a linear change in refractive index until a pressure is reached when the glass becomes birefringent. The glass continues to densify until the structure collapses and irreversible damage begins to form. If the pressure pulse amplitude and shape did not change it could be expected that the same propagation velocity were observed with the shadowgraph and the crossed polarizers arrangement. Due to the specimen geometry a sequence of pressure pulses is formed, caused by partial reflections of the first pulse at the

surfaces and by the reflection of the transversal waves which are drawn along the surfaces. This phenomenon was also observed and described with the edge-on impact tests in different types of glass (*12*). Beinert demonstrated that energy is continuously transferred from the first pressure pulse to the next one and therefore the amplitude decreases steadily. The decreasing amplitude together with the shape of the pulses could explain the seemingly different velocities, since it can be assumed that the sensitivity of the two optical set-ups is different. Analysis of these results and interpretations are still on going.

2.2 Results With AlON

AlON specimens of 10-mm thickness and two specimens of 25-mm thickness with lateral dimensions 100 × 100 mm were delivered for impact testing to EMI. The flat surfaces of the specimens and all the edges were polished in order to enable observation with high-speed cameras from all directions. However, it turned out that due to light scattering it was not possible to get a clear view through a thickness of 100 mm (from edge to edge). Therefore, the pictures recorded with the top view camera did not show any details of the damage progression inside the specimens. Those pictures could be used to control the impact position of the projectile, especially in the tests where the powder gun was used, so that the projectile hit the specimen after a free flight over a distance of 170 cm.

The tests with AlON were conducted in the velocity range from 250 to 950 m/s. The test matrix is given in table 3. As with the fused silica, the tests with AlON were performed in pairs of shots at the same nominal velocity, whereas one test was conducted in the shadowgraph configuration and the other test with the crossed polarizers set-up. The nominal impact velocities were 270, 380, 600, and 850 m/s.

Table 3. Test matrix with AlON.

Test No.	Impact Vel. (m/s)	Set-up	Cameras	Time Intervals	
14894	278	No polarizers	2	1-20: 0.5 µs	—
14895	270	Cr. polarizers	2	1-20: 0.5 µs	—
14897	381	No polarizers	2	1-18: 0.5 µs	18-20: 1 µs
14898	368	Cr. polarizers	2	1-18: 0.5 µs	18-20: 1 µs
14906	820	No polarizers	2	1-18: 0.5 µs	18-20: 1 µs
14907	925	Cr. polarizers	2	1-18: 0.5 µs	18-20: 1 µs
14908	588	No polarizers	2	1-18: 0.5 µs	18-20: 1 µs
14909	664	Cr. polarizers	2	1-18: 0.5 µs	18-20: 1 µs
14923	390	No polarizers inhomog. spec.[a]	2	1-16: 0.5 µs	16-20: 1 µs
14924	385	No polarizers spec. with defect	2	1-16: 0.5 µs	16-20: 1 µs
14925	385	No polarizers 25-mm specimen	2	1-16: 0.5 µs	16-20: 1 µs
14940	397	No polarizers reflected light	1	1-20: 0.5 µs	—

[a]Inhomogeneous specimen.

The results with test nos. 14894, –895, –897, –898, and 14940 were described and analyzed in the second interim report and partly published at the 22nd International Symposium on Ballistics (*13*). Therefore, this report focuses on the analysis of the EOI-tests at high impact velocities (14906–14909), tests with specimens with inhomogenieties (14923, 14924), and a test with a specimen of 25-mm thickness.

2.2.1 Tests at High-Impact Velocities

In order to achieve impact velocities between 400 and 950 m/s, a 30-mm powder gun with a rifled barrel had to be used for the acceleration of the projectiles. Due to the muzzle flash and the fumes the specimens could not be placed in a short distance to the muzzle. In those cases the distance between the muzzle and the specimens was 170 cm. The use of the powder gun and the type of projectile (steel cylinder with steel guidance band for transfer of twist) caused a relatively high scatter in the muzzle velocity.

2.2.1.1 Test Nos. 14906/14907; v_P = 820/925 m/s. Figure 2 shows a selection of four shadowgraphs and the corresponding crossed polarizers photographs at impact velocities of 820 and 925 m/s, respectively.

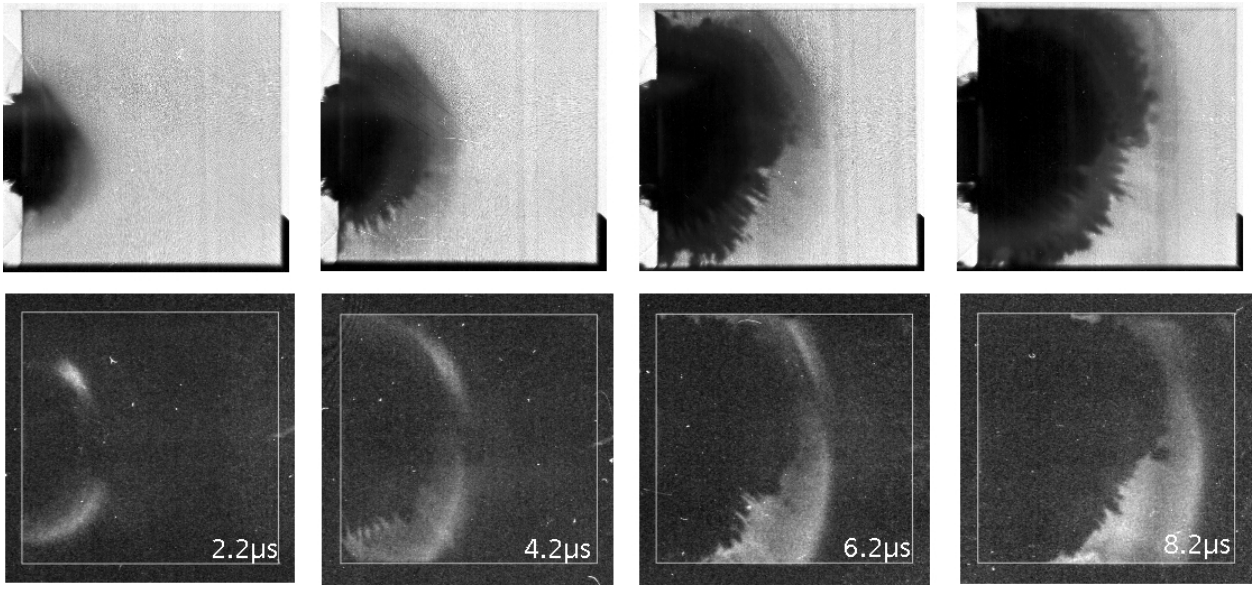

Figure 2. Selection of four shadowgraphs and corresponding crossed polarizers photographs from impact on AlON.

The series of high-speed photographs shows rapidly growing darkened to opaque regions, which reflect changes in the optical transmission due to pressure induced refractive index changes, damaged and fractured zones within the specimen. In addition, the nucleation of crack centers ahead of the crack front is clearly visible 6.2 and 8.2 µs after impact. In contrast to the shadowgraphs, where a wave front is not clearly discernable, the crossed polarizers configuration reveals an approximately semicircular wave front which is a little further advanced compared to

the damage front visible in the shadowgraphs at the same time. The complete series of photographs are shown in the appendix (figures A-1 and A-2).

Figure 3 illustrates path-time data of wave and damage/fracture propagation for the two tests. The data of the wave propagation, determined from the crossed polarizers test, are represented by the red filled circles. Two linear regions with different slopes can be distinguished.

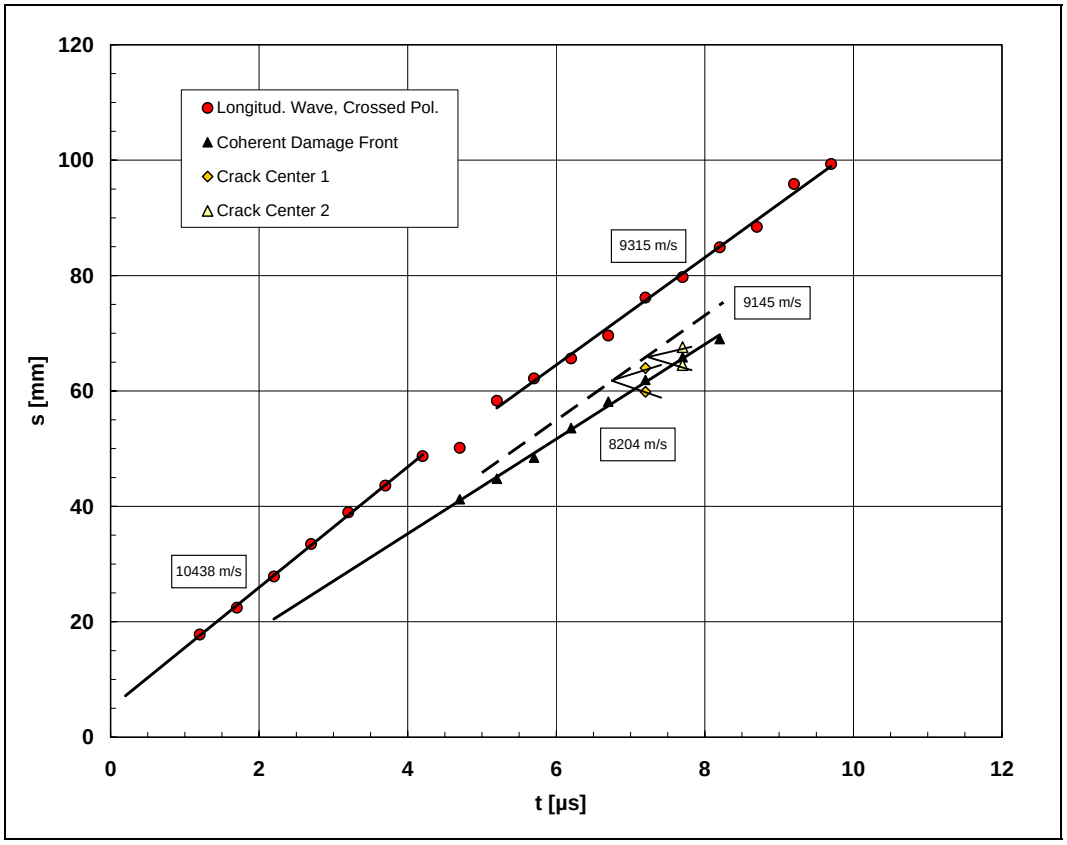

Figure 3. Path-time data of wave and fracture propagation at impact velocities of 820 and 925 m/s.

Linear regression of the data from 1.2 to 4.2 µs yields an average wave speed of 10,438 m/s, which approximately corresponds to the longitudinal wave speed of 10,300 m/s determined by means of ultrasonic wave measurements. Between 4 and 5 µs after impact, a deceleration of the wave speed seems to occur, whereas after 5 µs a linear section is observed again. Linear regression of that part of the data yields an average wave speed of 9315 m/s. The phenomenon of an apparent deceleration, followed by another linear section, was already observed more distinctly in AlON with the damage front in the tests at lower impact velocities (*7*). This optical effect was denoted birefringence shift and was attributed to the stress induced birefringence. However, it is not clear yet why a change in the average wave speed is observed. The complete series of high-speed photographs from the crossed polarizers set-up (see figure A-2) shows that during the first 4.2 µs, the stress wave front, which appears bright on the photographs, is not

visible in the centre. From picture no. 9 (4.7 µs), the stress wave front forms a coherent bright zone. This suggests a correlation between the appearance of the stress wave front and the measured velocity. In the tests at lower impact velocities a coherent stress wave front was visible in nearly all the photographs and split-up in sections with different slopes was not observed. The major difference between the high and low velocity tests, with respect to the impact conditions, is the accuracy. The projectile is still guided in the barrel of the gas gun for impact velocities below 450 m/s, whereas the free flight distance of 170 cm at high impact velocities allows yawing of the projectile and an off-set from the axis through the gun barrel and the specimen. This is illustrated in figure 4, which shows a top view of the impacted specimen from test nos. 14906 and 14909.

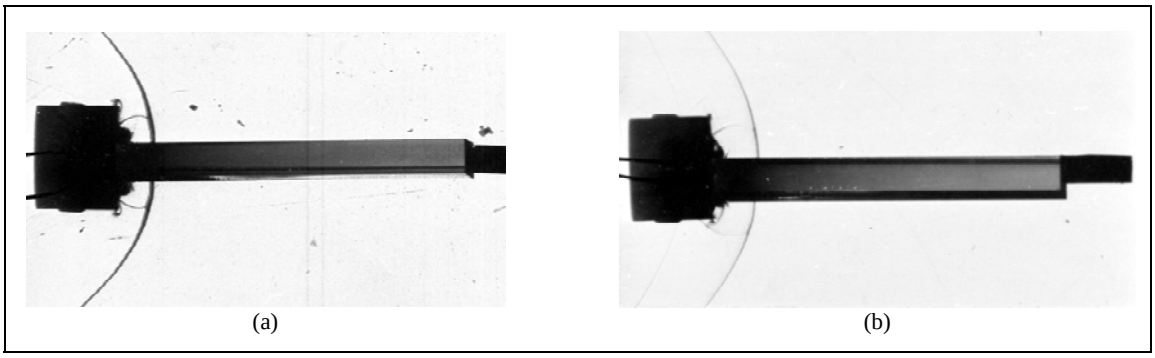

Figure 4. (a) Test no. 14906, top view, t = 0.7 µs and (b) test no. 14909, top view, t = 0.7 µs.

As the side-view photographs of test no. 14906 show (figure A-1), yaw of the projectile in the vertical plane (parallel to the 100 mm-square surfaces) results in an asymmetric formation of the damage front. Yaw in the horizontal plane, perpendicular to the 100-mm square surfaces, also strongly affects wave propagation in the specimen. Since the thickness of the specimen is only 10 mm, yaw of the projectile can cause a multitude of reflections and superposition of waves, which can affect the stress states and the visibility of the stress wave front.

Considering the velocity of the coherent damage front, which grew at an average velocity of 8204 m/s, no significant differences to the low velocity impact tests were observed. The number of crack centers ahead of the coherent fracture front was not significantly higher with the high impact velocity. The damage velocity, determined by linear regression through the nucleation sites of the crack centers, was 9145 m/s (dashed line, figure 3).

2.2.1.2 Test Nos. 14908/14909; v_P = 588/664 m/s. Figure 5 shows a selection of four shadowgraphs and the corresponding crossed polarizers photographs at impact velocities of 588 and 664 m/s, respectively. The complete series of photographs are shown in the appendix (figures A-3 and A-4).

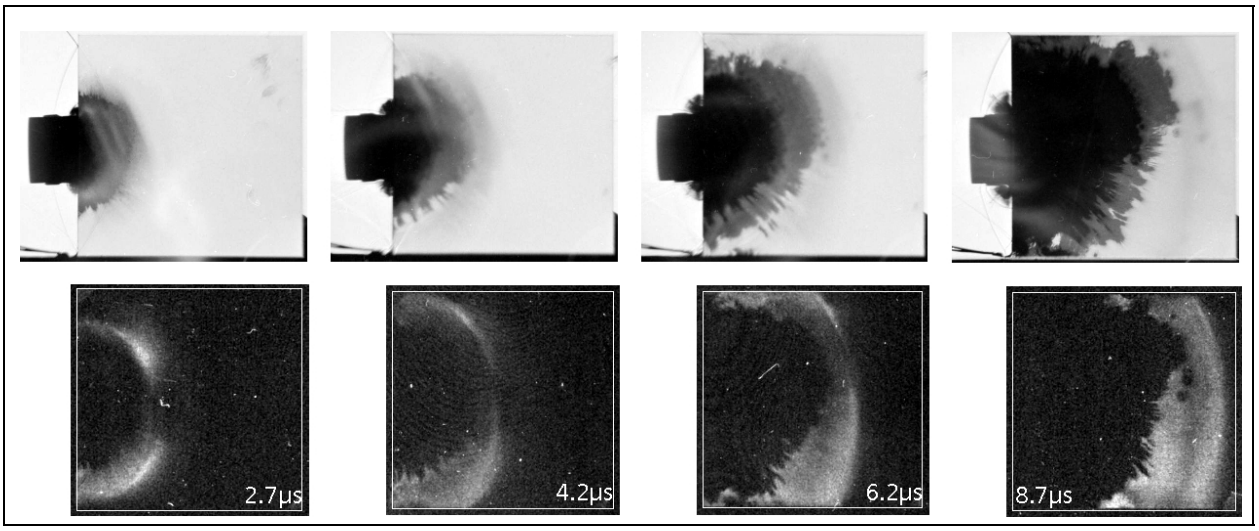

Figure 5. Selection of four shadowgraphs and corresponding crossed polarizers photographs from impact on AlON.

Considering fracture formation, the high-speed photographs basically show the same characteristics as observed at other impact velocities. The positions of the wave front, fracture front, and the crack centers are plotted vs. time in figure 6. The average velocity of the coherent fracture front was 8413 m/s. The development of five crack centers could be observed and linear regression through the nucleation points yields a damage velocity of 8976 m/s.

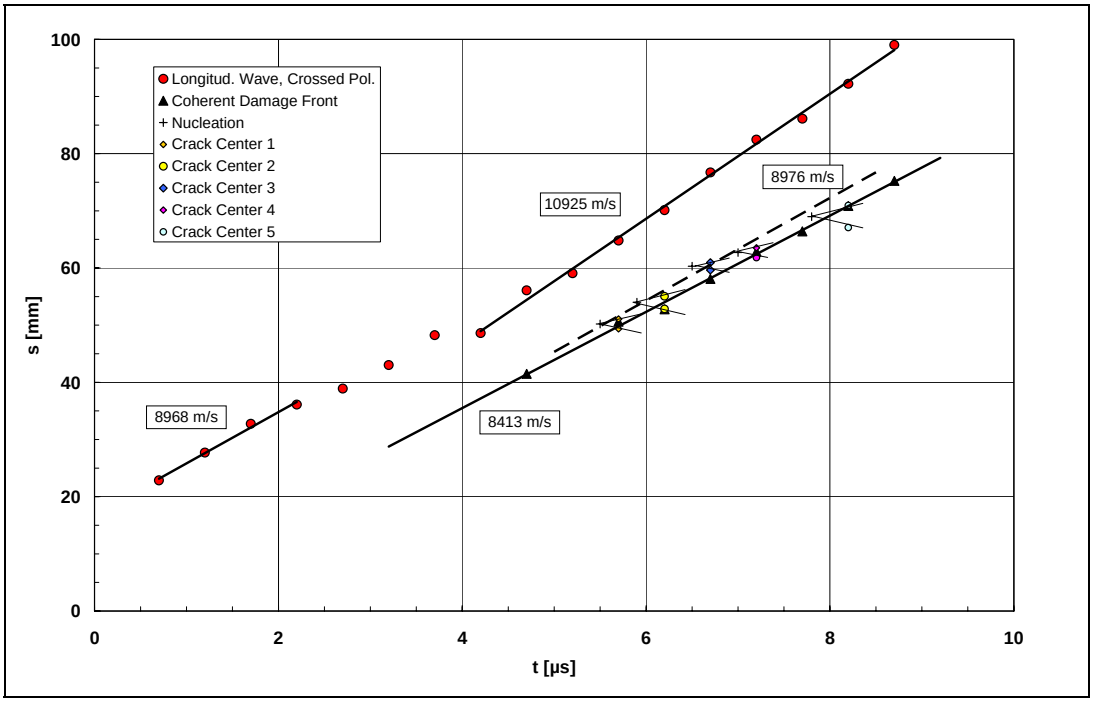

Figure 6. Path-time data of wave and fracture propagation at impact velocities of 588 and 664 m/s.

As observed in test no. 14907, sections with different slopes (wave velocities) can be distinguished. The most obvious change is again observed at about 4 µs. However, in this test a lower wave propagation velocity (8968 m/s) is observed before 4 µs and a higher velocity (10,925 m/s) after 4 µs. The most striking feature of the wave position data during the first microseconds is the high off-set. In order to reach the measured positions the wave velocity would have to be unrealistically high during the first microsecond after impact. Therefore, it appears more plausible that the off-set is either due to birefringence shift or to a delayed trigger signal, caused by a slightly inclined impact of the projectile as can be seen from the top view photograph in figure 4(b).

2.2.2 Tests With Inhomogeneous Specimens

An optical inspection of the specimens between crossed polarizers on a light box revealed inhomogenieties of the material in some cases. Figure 7 shows a specimen of 10-mm thickness on a light box with one sheet polarizer under the specimen (left) and between two crossed polarizers (right). The picture with the crossed polarizers reveals four zones where light passes through the specimen, arranged symmetrically like four petals of a blossom, directed towards the corners of the AlON specimen. This phenomenon was observed clearly with both specimens of 25-mm thickness, with two specimens of 10-mm thickness, and it could be seen faintly with a few other specimens. It is assumed that it is connected to internal stresses due to an inhomogeneous temperature distribution in the furnace during sintering and cooling.

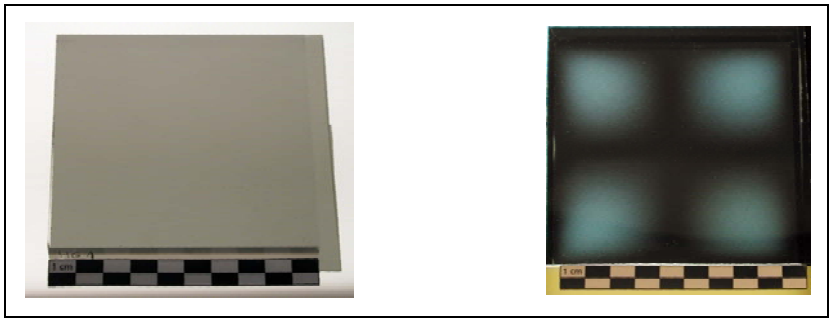

Figure 7. Specimen with inhomogenieties on a light box with one polarizer beneath (left) and between crossed polarizers (right).

One specimen with inhomogenieties as just described was tested at 390 m/s in a shadowgraph configuration. Figure 8 shows a selection of eight photographs from this test. The complete series of photographs is presented in figure A-5 of the appendix.

The photographs illustrate that no influence of the inhomogenieties on fracture formation was found. The same phenomena and a fracture front velocity of the same order of magnitude as in other tests at similar conditions were observed. This is demonstrated by the path-time histories plotted in figure 9. The front that was observed during the first 4 µs propagated at an average

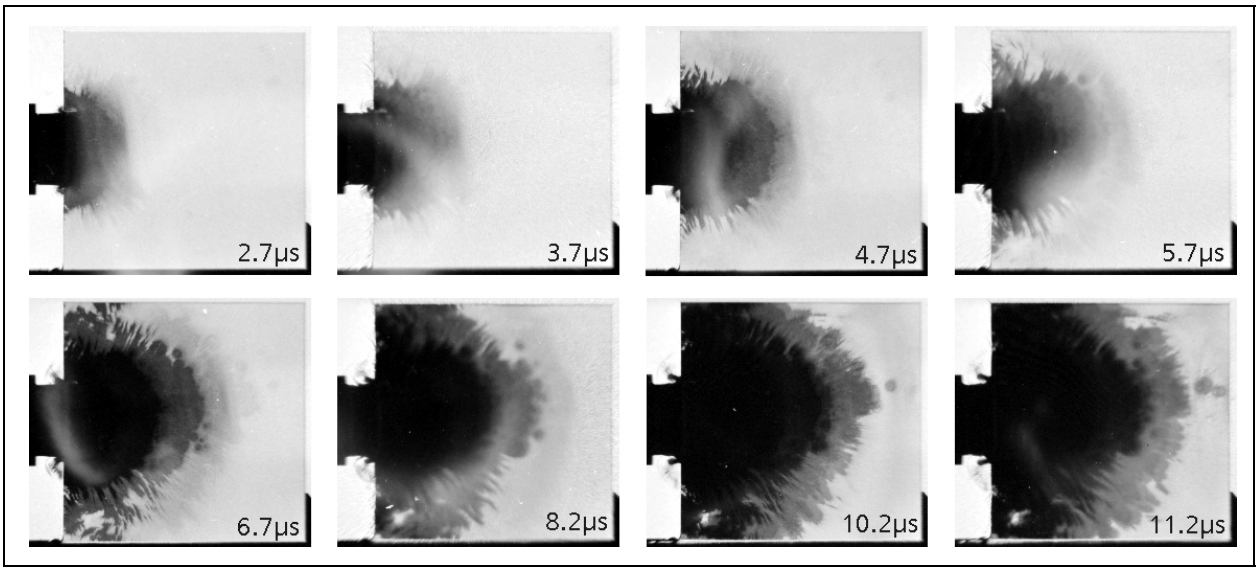

Figure 8. Selection of eight shadowgraphs from impact on inhomogeneous AlON specimen, test no. 14923, v_P = 390 m/s.

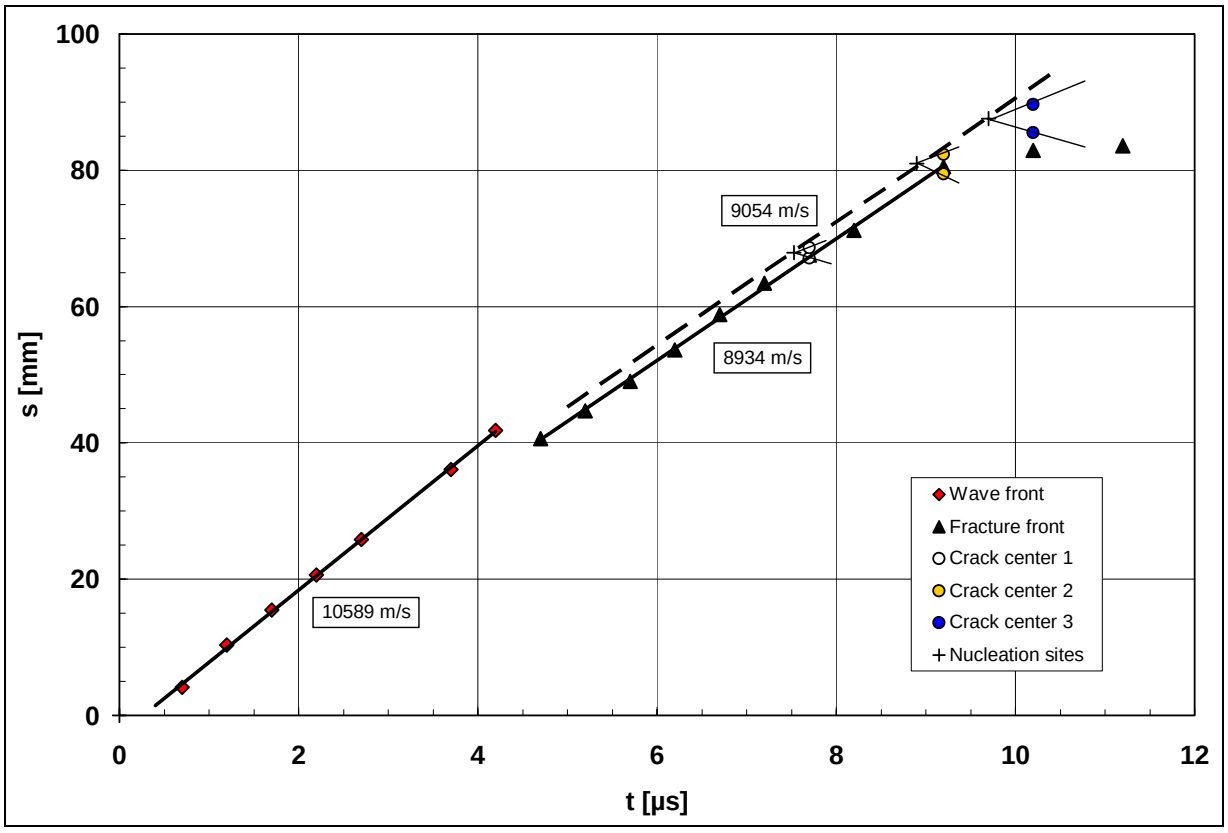

Figure 9. Path-time data of wave and fracture propagation in inhomogeneous specimen (internal stress), impacted at 390 m/s.

velocity of 10,589 m/s, which corresponds to the longitudinal wave velocity. The average speed of the coherent fracture front was 8934 m/s. Considering the crack centers ahead of the coherent fracture front, a damage velocity of 9054 m/s could be determined.

One AlON specimen of 10-mm thickness contained a flaw that was visible to the naked eye. It was not possible to determine the nature of the flaw, but from its appearance it could be concluded that it was either a small bubble or inclusion in the interior of the tile. However, the flaw was not visible in the high-speed photographs. The specimen was also tested at an impact velocity of ≈ 400 m/s. Figure 10 shows a selection of eight photographs from this test. The complete series of photographs is presented in figure A-6 of the appendix.

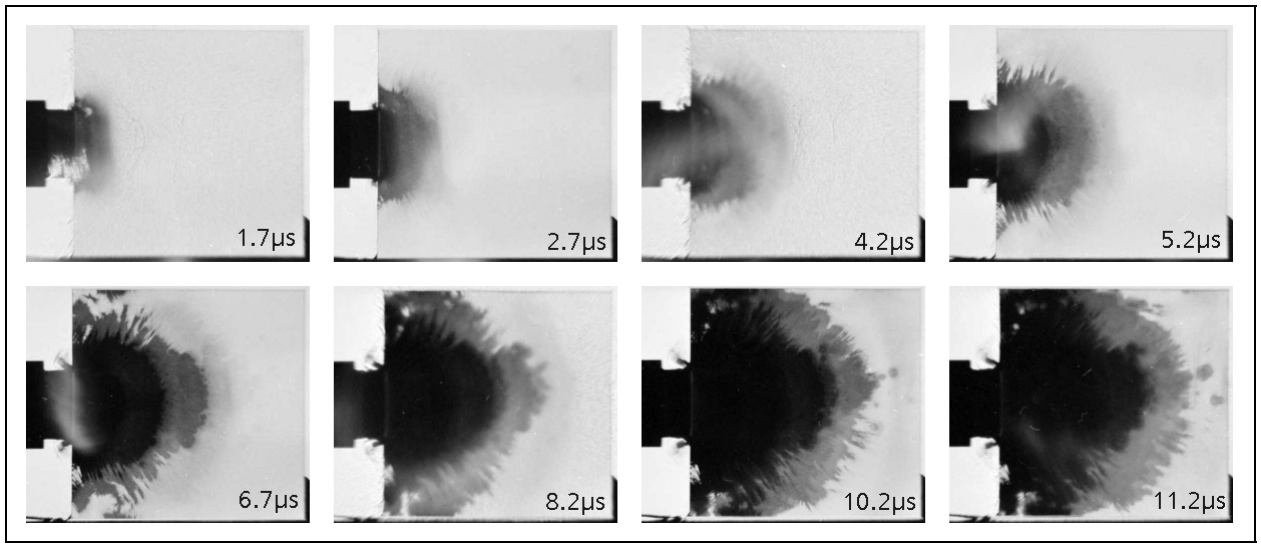

Figure 10. Selection of eight shadowgraphs from impact on inhomogeneous AlON specimen, test no. 14924, v_P = 385 m/s.

From the view of the camera the position of the flaw was in the upper left quadrant of the specimen. It was expected that the flaw might act as a nucleation site for damage on the arrival of the stress wave. The photographs in figure 10 demonstrate that this hypothesis could not be confirmed. The same phenomena as in test no. 14923 were observed and the coherent fracture front velocity of 8918 m/s was nearly equal to fracture front velocity determined in the previous test at 390 m/s. The time dependent progress of the wave and fracture front is illustrated in figure 11. During the first 6 μs a wave front was observed which propagated at an average speed of 10,594 m/s. Considering the crack centers ahead of the coherent fracture front, a damage velocity of 9145 m/s could be determined.

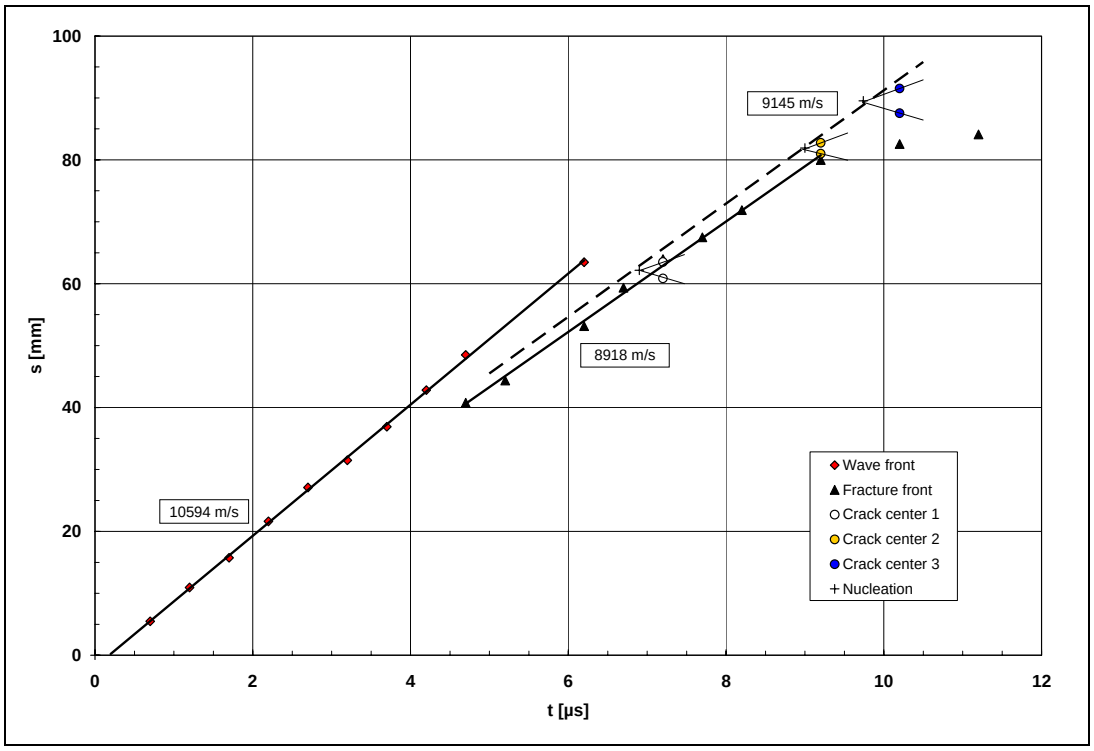

Figure 11. Path-time data of wave and fracture propagation in specimen with flaw, impacted at 385 m/s.

2.2.3 Test With Specimen of 25-mm Thickness

In order to test the influence of specimen thickness on damage formation one experiment was conducted with a specimen of 25-mm thickness. The specimen also exhibited the kind of inhomogeneity as described with the specimen of test no. 14923 (see figure 7). Figure 12 shows a selection of eight photographs from this test. The complete series of photographs is presented in figure A-7 of the appendix.

The photographs in figure 12 illustrate that the same phenomena occur in the thick specimen as were observed in the 10-mm specimens. The most advanced front that could be recognized propagated at an average velocity of 10,478 m/s and thus was identified as a longitudinal wave. Compared to the 10-mm specimens, the wave front was much better discernible in the thick specimen. In contrast to the wave front, the tip of the fracture front was hardly discernible in most of the photographs. Only three photographs allowed an accurate measurement of the fracture front position. The average velocity determined from these data was 8256 m/s.

The path-time histories of the wave and fracture front are depicted in figure 13. The blurred appearance of the fracture front is attributed to the enhanced scatter of light, due to the higher thickness of the specimen on one hand. On the other hand, the effect of birefringence shift is stronger with the thicker specimen.

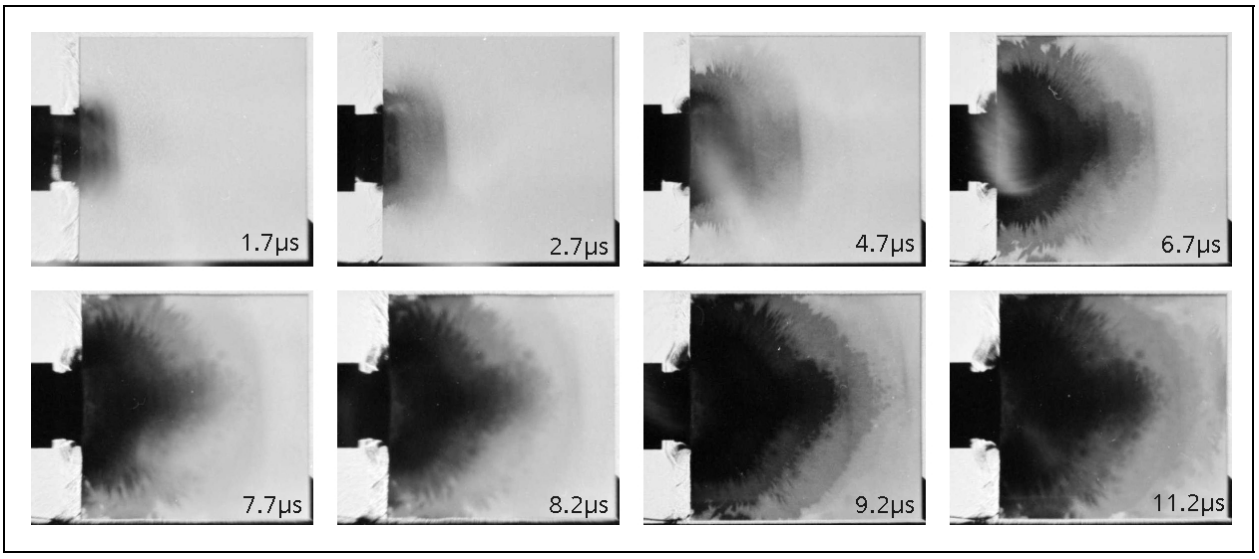

Figure 12. Selection of eight shadowgraphs from impact on AlON specimen of 25-mm thickness, test no. 14925, v_P = 385 m/s.

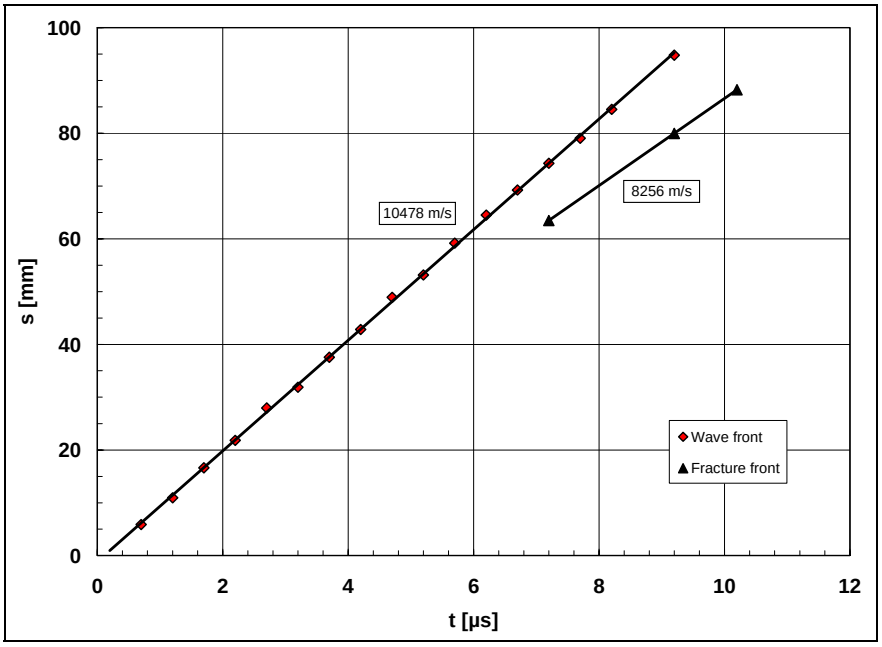

Figure 13. Path-time data of wave and fracture propagation in specimen of 25-mm thickness, impacted at 385 m/s.

2.2.4 Summary of Results With AlON

A compilation of the measured stress wave, coherent fracture front, and damage velocities is given in table 4. The coherent fracture front velocities were all in the range from 8000 to 9400 m/s, whereas the damage velocities ranged from 8900 to 9800 m/s. The damage velocities are presented as a function of impact velocity in figure 14 along with the data of other types of armor ceramics.

Table 4. Compilation of wave and fracture velocity data with AlON.

Test No.	Impact Vel. (m/s)	Optical Set-up	Stress Wave Velocity (m/s)	Coh. Fracture Front Velocity (m/s)	Damage Velocity (m/s)
14894	278	Shadowgraph	—	7994/8081	9066
14895	270	Cr. polarizers	9944	—	—
14897	381	Shadowgraph	—	8381	9156
14898	368	Cr. polarizers	9367	—	—
14906	820	Shadowgraph	—	8204	9145
14907	925	Cr. polarizers	10438/9315	—	—
14908	588	Shadowgraph	—	8413	8976
14909	664	Cr. polarizers	8968/10925	—	—
14923	390	Shadowgraph	10589	8934	9054
14924	385	Shadowgraph	10594	8918	9145
14925	385	Shadowgraph	10478	8256	—
14940	397	Reflected light	10564	9361	9767

In each of the ceramics the damage velocity increases with rising impact velocity. The damage velocities approach the longitudinal wave velocity c_L at high loadings. With most of the materials a steep rise of v_D is observed in the range of impact velocities between 150 and 200 m/s. Since all tests with AlON were conducted at impact velocities above 250 m/s high damage velocities had been expected. The damage velocities were all in the range from 85% to 95% of the longitudinal wave velocity, which corresponds to the results with aluminum oxide.

3. Conclusion

- The edge-on impact technique was modified in order to visualize stress wave propagation in transparent ceramics. The specimens were placed between crossed polarizers and the photo-elastic effect was successfully utilized to visualize the stress waves.
- Pairs of impact tests at approximately equivalent velocities were carried out in transmitted plain (shadowgraphs, visualization of damage) and crossed polarized light (visualization of wave propagation).

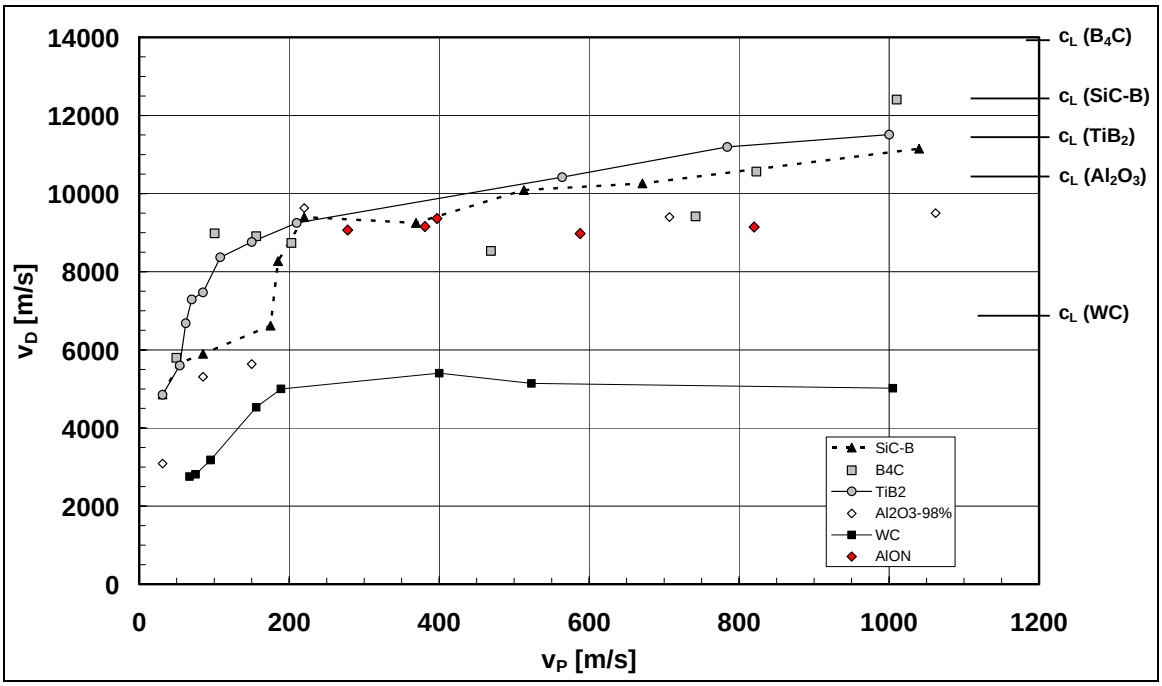

Figure 14. Damage velocity v_D vs. impact velocity v_P for different armor ceramics.

- The experiments provided direct evidence of ceramic damage by nucleation and growth of fracture initiated by the stress waves, ahead of the coherent fracture front growing from the impacted edge.
- A comparison of the results in a reflected light set-up and the shadowgraphs indicated fracture nucleation in the interior of the ceramic.
- The experimental results provide a data basis for a deeper analysis of the damage mechanisms by means of numerical simulation.

4. References

1. Senf, H.; Straßburger, E.; Rothenhäusler, H. Stress Wave Induced Damage and Fracture in Impacted Glasses. *Journal Phys. IV, C8* **1994**, *4*, 741–746.

2. Senf, H.; Straßburger, E.; Rothenhäusler, H. Visualization of Fracture Nucleation During Impact in Glass. *Metallurgical and Materials Applications of Shock-Wave and High-Strain-Rate Phenomena* **1995**, 163–170.

3. Straßburger, E. Visualization of Impact Damage in Ceramics Using the Edge-On Impact Technique. *Int. Journal of Applied Ceramic Technology, Topical Focus: Ceramic Armor, The American Ceramics Society* **2004**, *1* (3), 235–242.

4. Senf, H.; Straßburger, E.; Rothenhäusler, H. A Study of Damage During Impact in Zerodur. *Journal Phys IV* **1997,** *7* (3), 1015–1020.

5. Patel, P. J.; Gilde, G. A. Transparent Armor Materials: Needs and Requirements. *Ceramic Transactions* **2001,** *134*, 573–586.

6. Straßburger, E. *High-Speed Photographic Study of Wave Propagation and Impact Damage in Transparent Aluminum Oxynitride (AlON)*; first interim report, contract no. N62558-04-P-6031, EMI Report E 29/04, November 2004.

7. Straßburger, E. *High-Speed Photographic Study of Wave Propagation and Impact Damage in Transparent Aluminum Oxynitride (AlON)*; second interim report, contract no. N62558-04-P-6031, EMI Report E 11/05, March 2005.

8. Straßburger, E.; Patel, P.; McCauley, J. W.; Templeton, D. W. High-Speed Photographic Study of Wave and Fracture Propagation in Fused Silica. *Proceeding of the 22nd Int. Symposium on Ballistics*, Vancouver, BC, Canada, 14–18 November 2005.

9. Vollkommer, H. *Schlierenoptische Untersuchung des Schneidenstoßes auf eine Plattenkante*; EMI-Report 1/67, Ernst-Mach-Institut, 1967.

10. Settles, G. S. *Schlieren and Shadowgraph Techniques: Visualizing Phenomena in Transparent Media*; Springer: Heidelberg, 2001.

11. Beinert, J. Schlierenoptische Untersuchungen zur Ausbreitung kurzer elastischer Impulse in Platten. Ph.D. Thesis, Fraunhofer-Institute for Mechanics of Materials, Freiburg, Germany, 1974.

12. Straßburger, E.; Senf, H. *Experimental Investigations of Wave and Fracture Phenomena in Impacted Ceramics and Glasses*; ARL-CR-214; re-publication of EMI-Report 3/94; U.S. Army Research Laboratory: Aberdeen Proving Ground, MD, 1995.

13. Straßburger, E.; Patel, P.; McCauley, J. W.; Templeton, D. W. Visualization of Wave Propagation and Impact Damage in a Polycrystalline Transparent Ceramic – AlON. *Proceedings 22nd Int. Symposium on Ballistics*, Vancouver, BC, Canada, 14–18 November 2005.

Appendix. Complete Sets of High-Speed Photographs

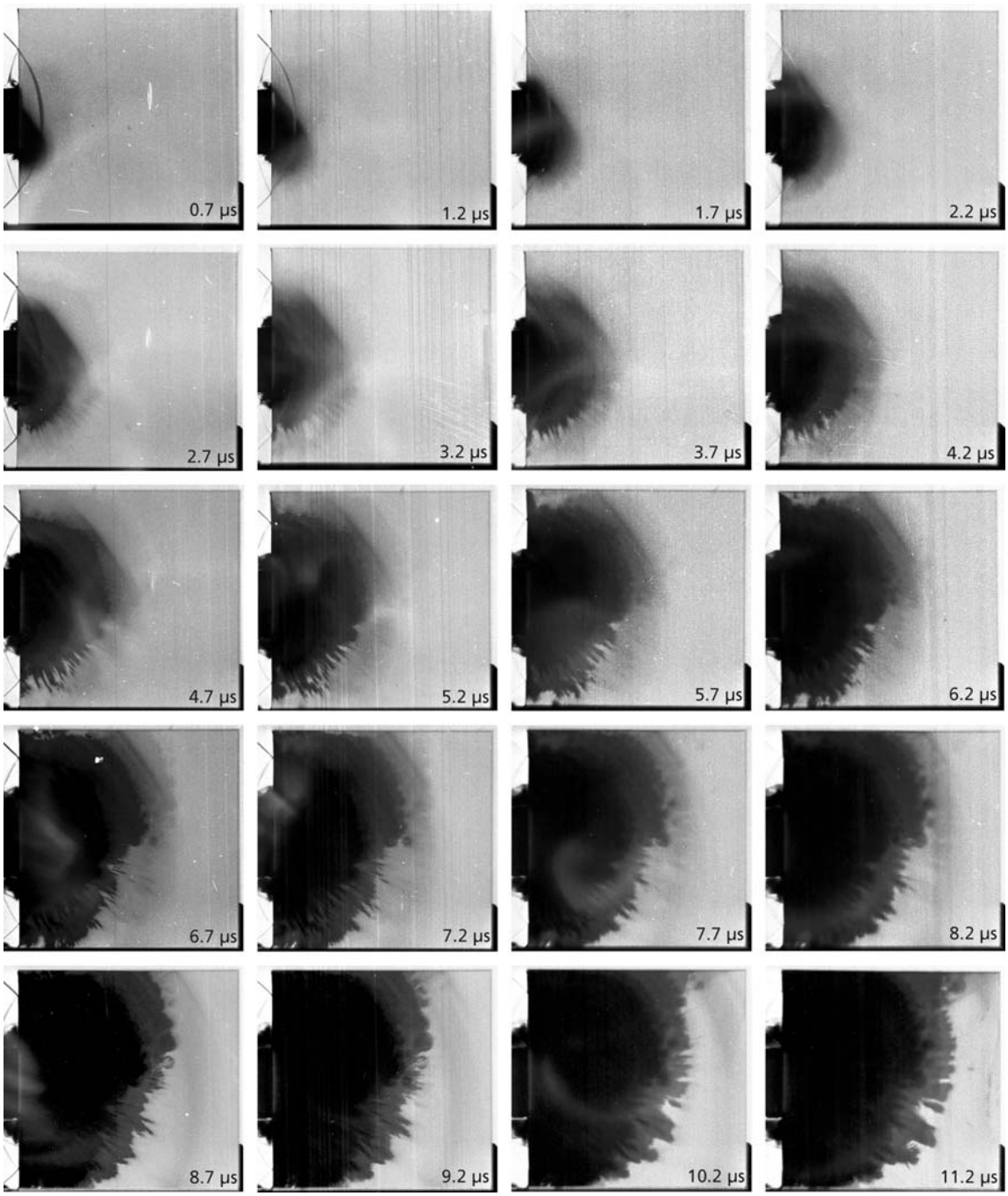

Figure A-1. High-speed photographs: shadowgraph arrangement, positive patterns, side-view test no. 14906, v_P = 820 m/s.

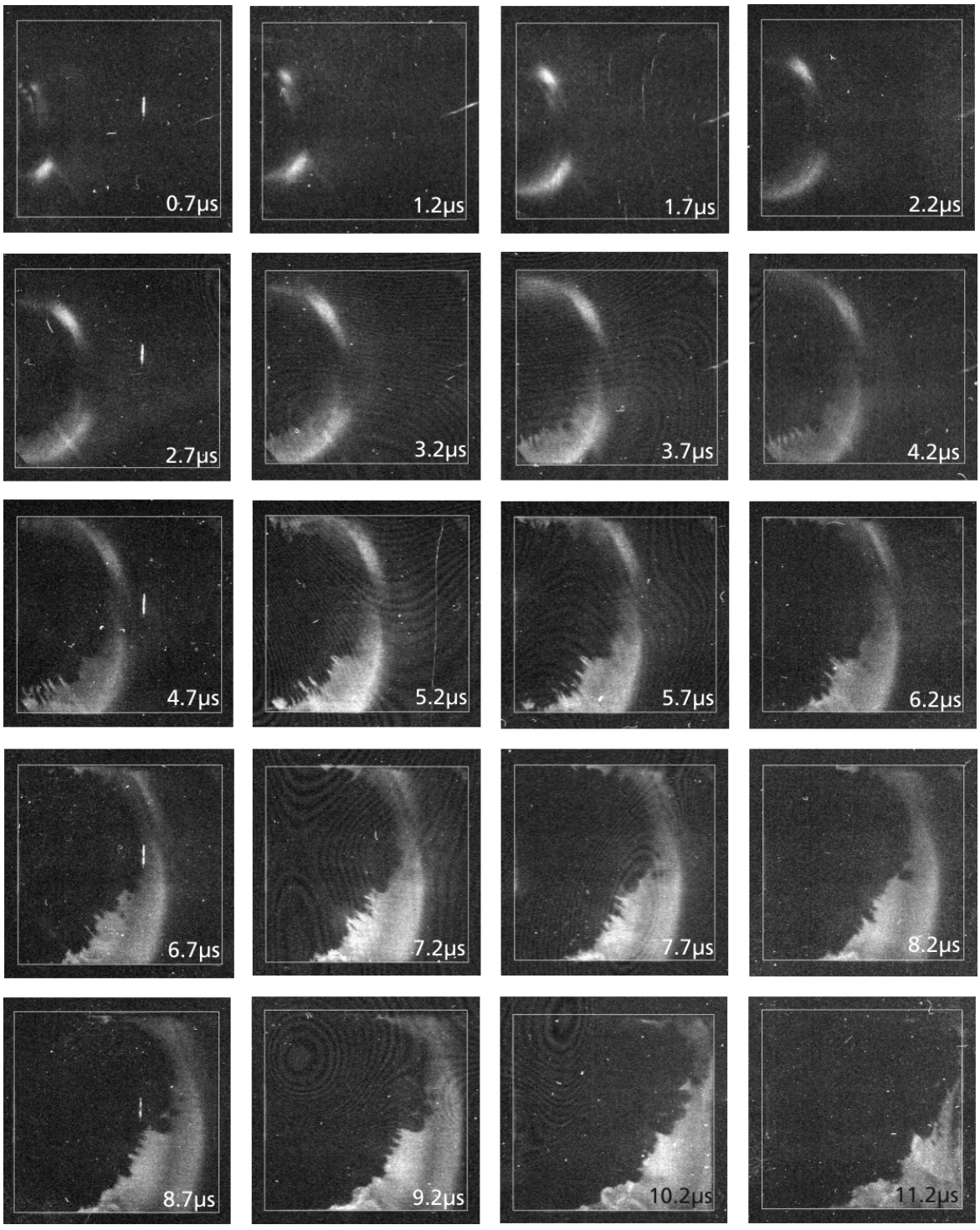

Figure A-2. High-speed photographs: crossed polarizers arrangement, positive patterns, side-view test no. 14907, v_p = 925 m/s.

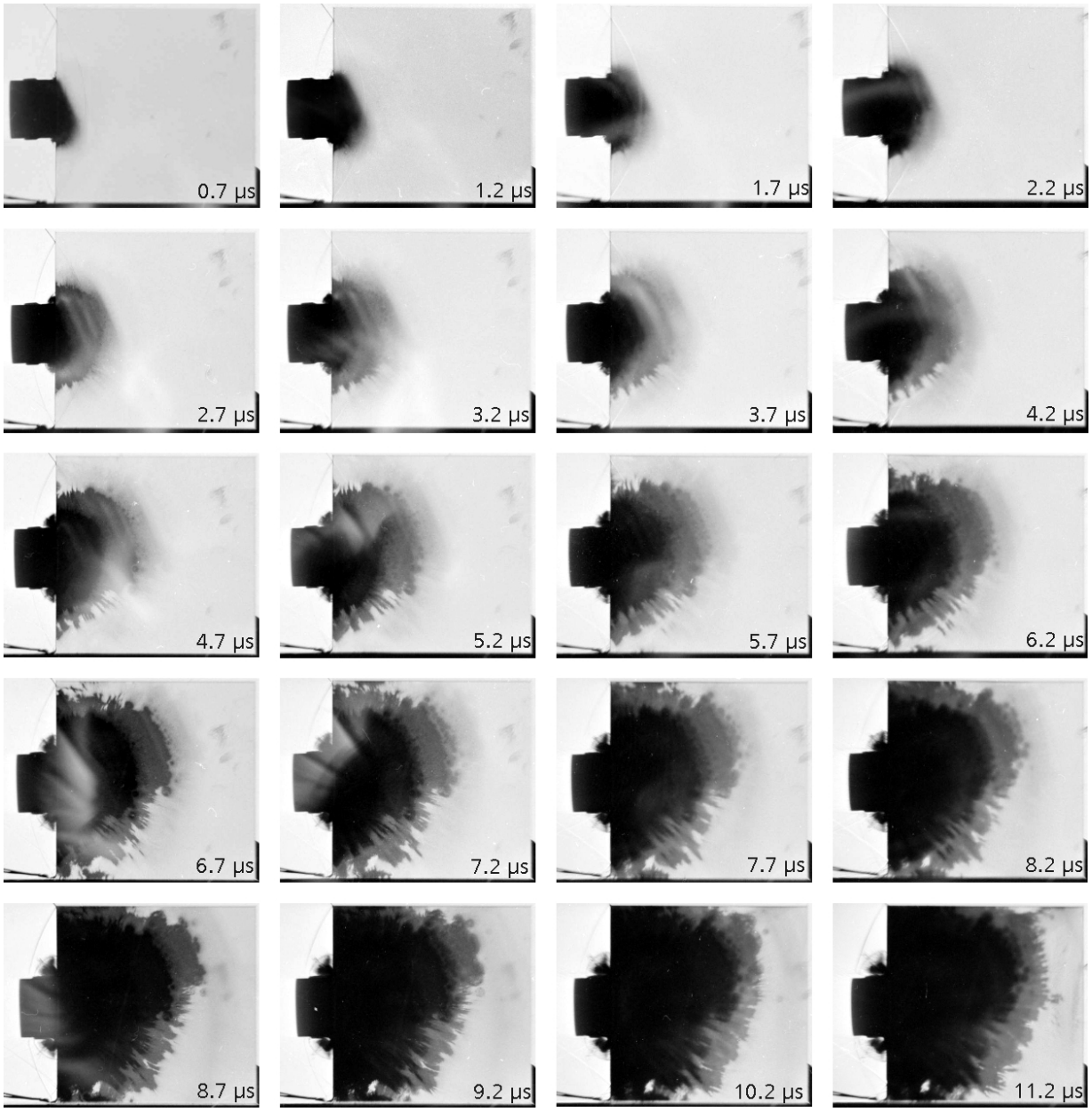

Figure A-3. High-speed photographs: shadowgraph arrangement, positive patterns, side-view test no. 14908, v_P = 588 m/s.

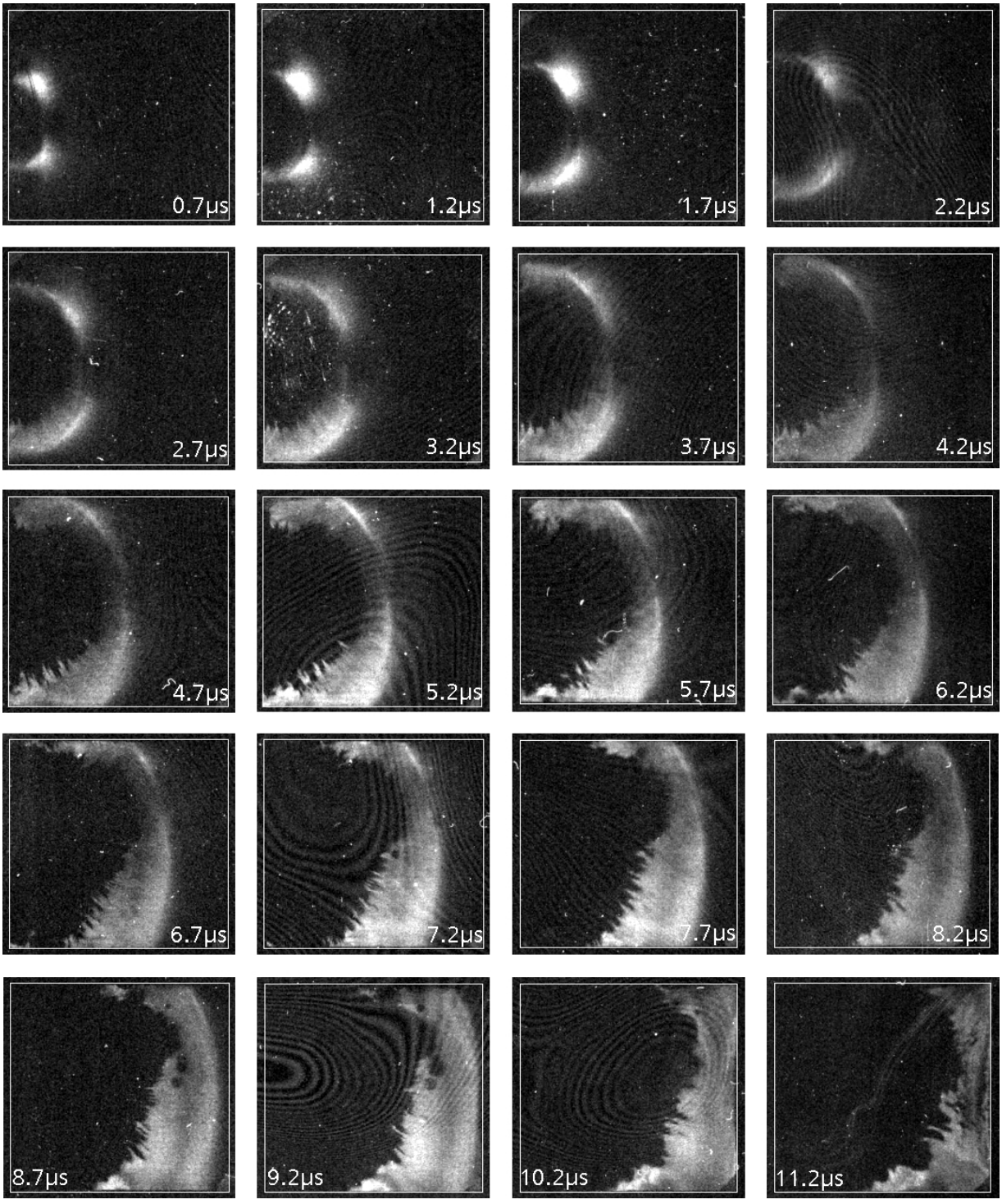

Figure A-4. High-speed photographs: crossed polarizers arrangement, positive patterns, side-view test no. 14909, v_p = 664 m/s.

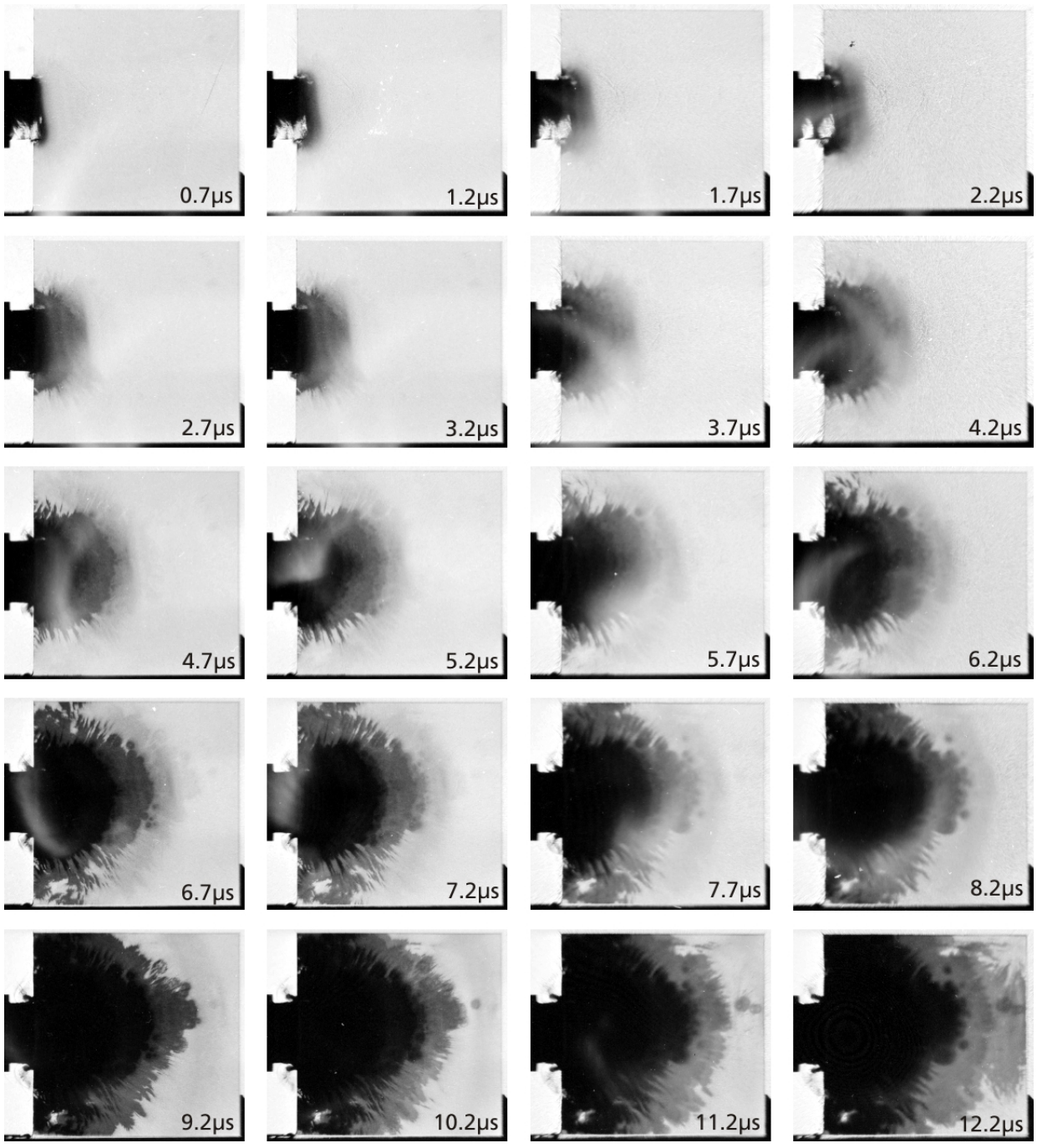

Figure A-5. High-speed photographs: shadowgraph arrangement, positive patterns, side-view inhomogeneous specimen; test no. 14923, v_P = 390 m/s.

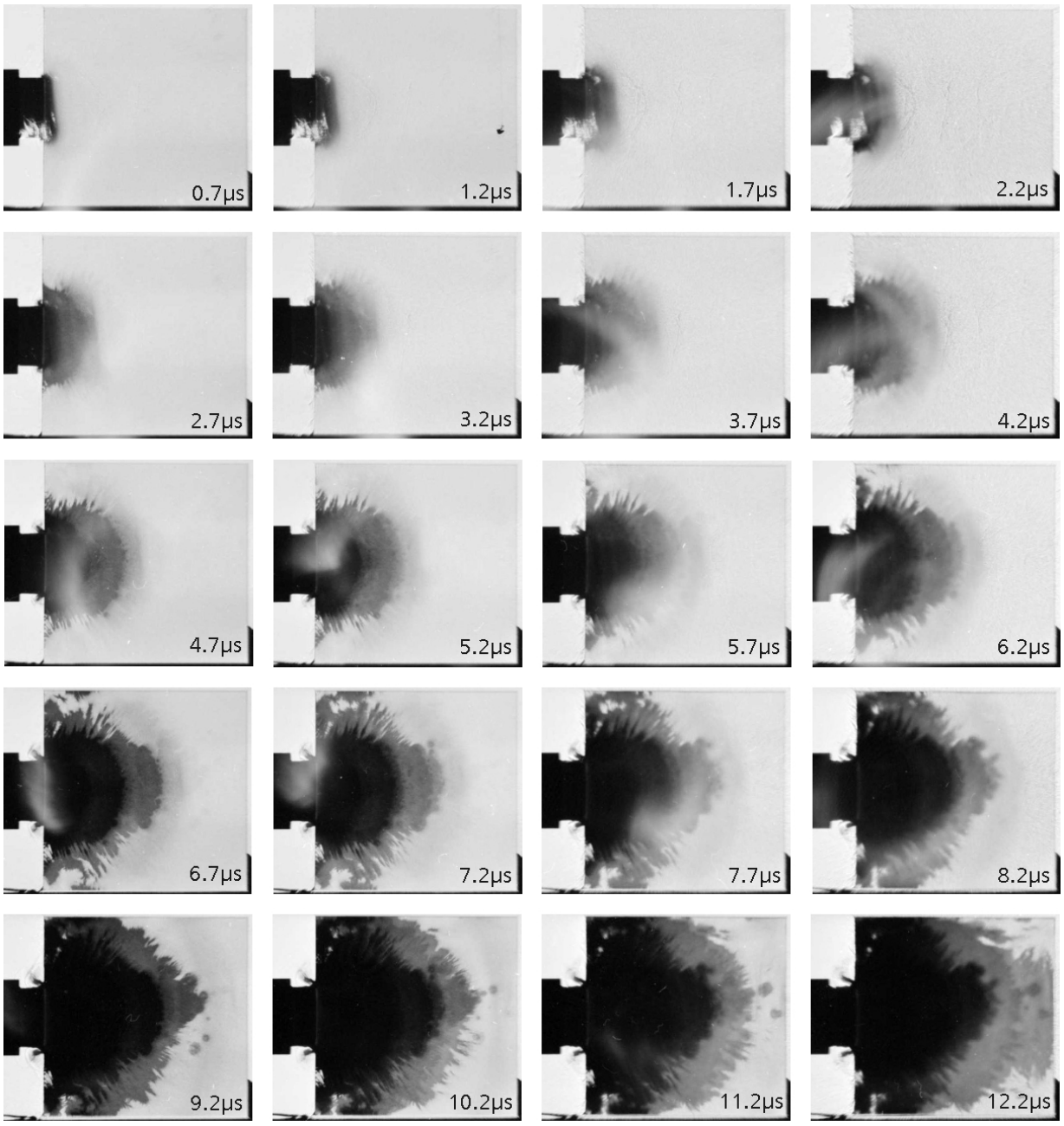

Figure A-6. High-speed photographs: shadowgraph arrangement, positive patterns, side-view specimen with flaw; test no. 14924, v_P = 385 m/s.

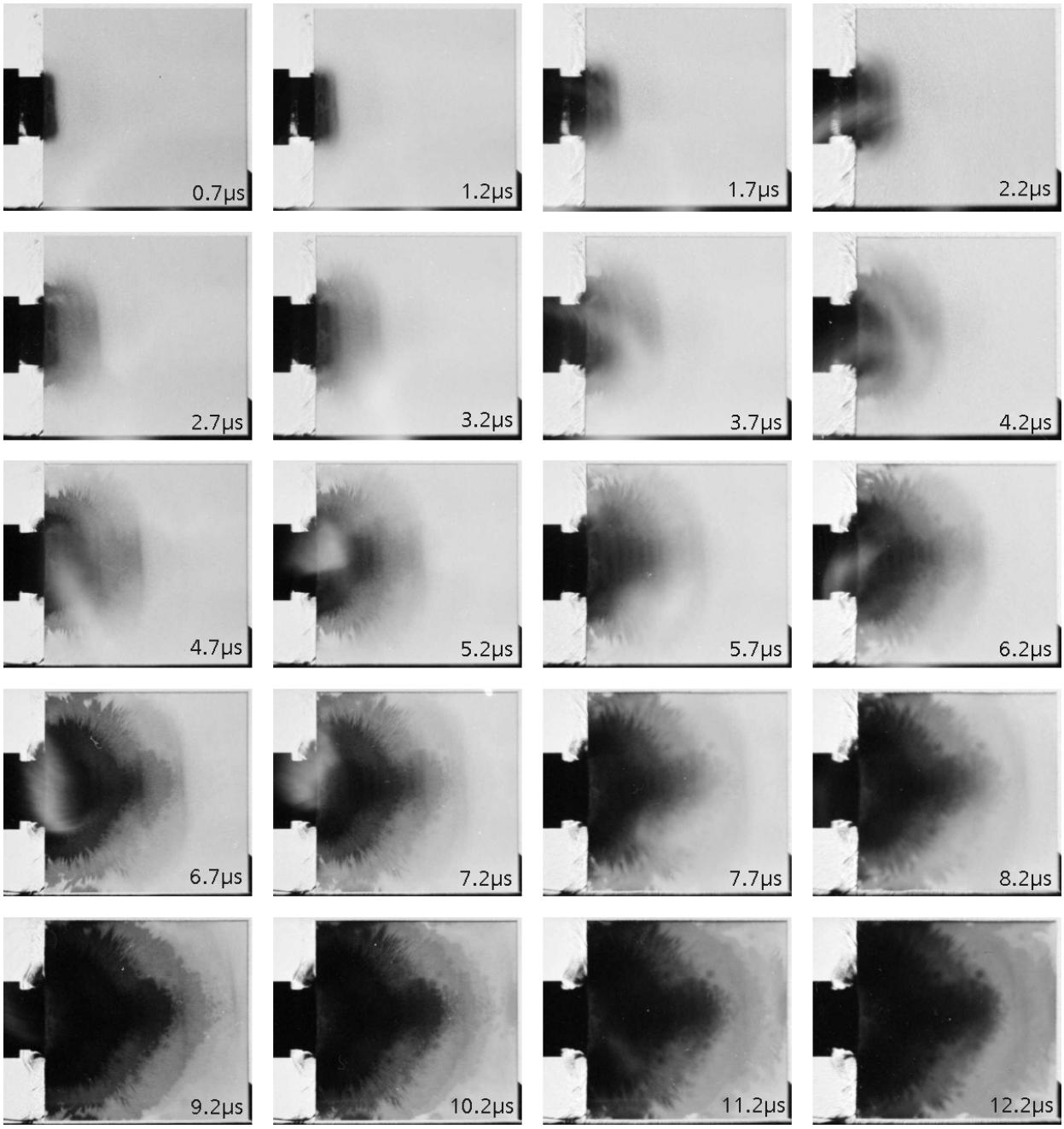

Figure A-7. High-speed photographs: shadowgraph arrangement, positive patterns, side-view specimen of 25-mm thickness; test no. 14925, v_P = 385 m/s.

NO. OF
COPIES ORGANIZATION

1 (PDF ONLY) DEFENSE TECHNICAL INFORMATION CTR
DTIC OCA
8725 JOHN J KINGMAN RD
STE 0944
FORT BELVOIR VA 22060-6218

1 US ARMY RSRCH DEV & ENGRG CMD
SYSTEMS OF SYSTEMS INTEGRATION
AMSRD SS T
6000 6TH ST STE 100
FORT BELVOIR VA 22060-5608

1 DIRECTOR
US ARMY RESEARCH LAB
IMNE ALC IMS
2800 POWDER MILL RD
ADELPHI MD 20783-1197

3 DIRECTOR
US ARMY RESEARCH LAB
AMSRD ARL CI OK TL
2800 POWDER MILL RD
ADELPHI MD 20783-1197

ABERDEEN PROVING GROUND

1 DIR USARL
AMSRD ARL CI OK TP (BLDG 4600)

NO. OF COPIES ORGANIZATION

1 DPTY ASST SECY FOR R&T
SARD TT
THE PENTAGON
RM 3EA79
WASHINGTON DC 20301-7100

1 COMMANDER
US ARMY MATERIEL CMD
AMXMI INT
9301 CHAPEK RD
FT BELVOIR VA 22060-5527

1 COMMANDER
US ARMY TACOM
PM HBCT
SFAE GCS HBCT S (MS 506)
6501 ELEVEN MILE RD
WARREN MI 48397-5000

1 COMMANDER
US ARMY TACOM
AMSTA SF
WARREN MI 48397-5000

1 OFC OF NAVAL RSRCH
J CHRISTODOULOU
ONR CODE 332
800 N QUINCY ST
ARLINGTON VA 22217-5600

1 COMMANDER
US ARMY TACOM
PM SURVIVABLE SYSTEMS
SFAE GCSS W GSI H
M RYZYI
6501 ELEVEN MILE RD
WARREN MI 48397-5000

1 COMMANDER
US ARMY TACOM
CHIEF ABRAMS TESTING
SFAE GCSS W AB QT
J MORAN
6501 ELEVEN MILE RD
WARREN MI 48397-5000

1 COMMANDER
WATERVLIET ARSENAL
SMCWV QAE Q
B VANINA
BLDG 44
WATERVLIET NY 12189-4050

NO. OF COPIES ORGANIZATION

2 HQ SFSJM CDL
US ARMY JOINT MUNITIONS CMD
AMSIO SMT
R CRAWFORD
W HARRIS
1 ROCK ISLAND ARSENAL
ROCK ISLAND IL 61299-6000

2 COMMANDER
US ARMY AMCOM
AVIATION APPLIED TECH DIR
J SCHUCK
FT EUSTIS VA 23604-5577

1 NAVAL SURFACE WARFARE CTR
DAHLGREN DIV CODE G06
DAHLGREN VA 22448

1 USA SBCCOM PM SOLDIER SPT
AMSSB PM RSS A
J CONNORS
KANSAS ST
NATICK MA 01760-5057

3 AIR FORCE ARMAMENT LAB
AFATL DLJW
W COOK
D BELK
J FOSTER
EGLIN AFB FL 32542

3 DPTY ASSIST SCY FOR R&T
SARD TT
ASA (ACT)
T KILLION
J PARMENTOLA
C CHABALOWSKI
THE PENTAGON RM 3E479
WASHINGTON DC 20310-0103

2 DARPA
W COBLENZ
L CHRISTODOULOU
3701 N FAIRFAX DR
ARLINGTON VA 22203-1714

3 DIRECTOR
US ARMY ARDEC
AMSTA AR FSA E
W DUNN
J PEARSON
E BAKER
PICATINNY ARSENAL NJ
07806-5000

NO. OF COPIES	ORGANIZATION
12	US ARMY TARDEC AMSTRA TR R MS 263 K BISHNOI D TEMPLETON (10 CPS) L FRANKS WARREN MI 48397-5000
1	COMMANDER US ARMY RSRCH OFC A RAJENDRAN PO BOX 12211 RSRCH TRIANGLE PARK NC 27709-2211
2	CALTECH G RAVICHANDRAN T AHRENS MS 252 21 1201 E CALIFORNIA BLVD PASADENA CA 91125
2	ARMY HIGH PERFORMANCE COMPUTING RSRCH CTR T HOLMQUIST G JOHNSON 1200 WASHINGTON AVE S MINNEAPOLIS MN 55415
3	SOUTHWEST RSRCH INST C ANDERSON J WALKER K DANNEMANN PO DRAWER 28510 SAN ANTONIO TX 78284
2	UNIV OF DELAWARE DEPT OF MECH ENGR J GILLESPIE NEWARK DE 19716
3	SRI INTERNATIONAL D CURRAN D SHOCKEY R KLOOP 333 RAVENSWOOD AVE MENLO PARK CA 94025
1	APPLIED RSRCH ASSOCIATES D GRADY 4300 SAN MATEO BLVD NE STE A220 ALBUQUERQUE NM 87110
1	INTERNATIONAL RSRCH ASSOCIATES INC D ORPHAL 4450 BLACK AVE PLEASANTON CA 94566
1	BOB SKAGGS CONSULTANT S SKAGGS 79 COUNTY RD 117 SOUTH SANTA FE NM 87501
2	WASHINGTON ST UNIV INST OF SHOCK PHYSICS Y GUPTA J ASAY PULLMAN WA 99164-2814
1	COORS CERAMIC CO T RILEY 600 NINTH ST GOLDEN CO 80401
1	UNIV OF DAYTON RSRCH INST N BRAR 300 COLLEGE PARK MS SPC 1911 DAYTON OH 45469
5	DIRECTOR USARL K WILSON FRENCH DEA 1396 ADELPHI MD 20783-1197
2	COMMANDER US ARMY TACOM AMSTA TR S T FURMANIAK L PROKURAT FRANKS WARREN MI 48397-5000
1	PROJECT MANAGER ABRAMS TANK SYSTEM J ROWE WARREN MI 48397-5000

NO. OF COPIES	ORGANIZATION
4	COMMANDER US ARMY RSRCH OFC B LAMATINA D STEPP W MULLINS D SKATRUD PO BOX 12211 RSRCH TRIANGLE PARK NC 27709-2211
1	NAVAL SURFACE WARFARE CTR CARDEROCK DIVISION R PETERSON CODE 28 9500 MACARTHUR BLVD WEST BETHESDA MD 20817-5700
4	LAWRENCE LIVERMORE NATL LAB R GOGOLEWSKI L290 R LANDINGHAM L369 J REAUGH L32 S DETERESA PO BOX 808 LIVERMORE CA 94550
6	SANDIA NATL LAB J ASAY MS 0548 R BRANNON MS 0820 L CHHABILDAS MS 0821 D CRAWFORD ORG 0821 M KIPP MS 0820 T VOLGER PO BOX 5800 ALBUQUERQUE NM 87185-0820
3	RUTGERS THE STATE UNIV OF NEW JERSEY DEPT OF CRMCS & MATLS ENGRNG R HABER 607 TAYLOR RD PISCATAWAY NJ 08854
1	NAVAL RSRCH LABORATORY CODE 6684 4555 OVERLOOK AVE SW WASHINGTON DC 20375
3	SOUTHWEST RSRCH INST C ANDERSON J RIEGEL J WALKER 6220 CULEBRA RD SAN ANTONIO TX 78238

NO. OF COPIES	ORGANIZATION
1	ARMORWORKS W PERCIBALLI 2495 S INDUSTRIAL PARK AVE TEMPE AZ 85281
1	CERCOM R PALICKA 991 PARK CENTER DR VISTA CA 92083
6	GDLS W BURKE MZ436 21 24 G CAMPBELL MZ436 30 44 D DEBUSSCHER MZ436 20 29 J ERIDON MZ436 21 24 W HERMAN MZ435 01 24 S PENTESCU MZ436 21 24 38500 MOUND RD STERLING HTS MI 48310-3200
1	INTERNATL RSRCH ASSN D ORPHAL 4450 BLACK AVE PLEASANTON CA 94566
1	JET PROPULSION LAB IMPACT PHYSICS GROUP M ADAMS 4800 OAK GROVE DR PASADENA CA 91109-8099
1	KAMAN SCIENCES CORP 1500 GARDEN OF THE GODS RD COLORADO SPRINGS CO 80907
3	OGARA HESS & EISENHARDT G ALLEN D MALONE T RUSSELL 9113 LE SAINT DR FAIRFIELD OH 45014
3	JOHNS HOPKINS UNIV DEPT OF MECH ENGRNG K T RAMESH 3400 CHARLES ST BALTIMORE MD 21218
1	SAIC J FURLONG MS 264 1710 GOODRIDGE DR MCLEAN VA 22102

NO. OF
COPIES ORGANIZATION

2 SIMULA INC
V HORVATICH
V KELSEY
10016 51ST ST
PHOENIX AZ 85044

6 UNITED DEFENSE LP
J DORSCH
B KARIYA
M MIDDIONE
R MUSANTE
R RAJAGOPAL
D SCHADE
PO BOX 367
SANTA CLARA CA 95103

3 UNITED DEFENSE LP
E BRADY
R JENKINS
J JOHNSON
PO BOX 15512
YORK PA 17405-1512

ABERDEEN PROVING GROUND

70 DIR USARL
AMSRD ARL WM
S KARNA
E SCHMIDT
J SMITH
T WRIGHT
AMSRD ARL WM BC
J NEWILL
AMSRD ARL WM M
S MCKNIGHT
R DOWDING
AMSRD ARL WM MC
R SQUILLACIOTI
AMSRD ARL WM MD
E CHIN
G GAZONAS
J LASALVIA
P PATEL
J MONTGOMERY
J SANDS
AMSRD ARL WM T
B BURNS
AMSRD ARL WM TA
P BARTKOWSKI
M BURKINS
W GOOCH
D HACKBARTH

NO. OF
COPIES ORGANIZATION

T HAVEL
C HOPPEL
E HORWATH
T JONES
M KEELE
D KLEPONIS
H MEYER
J RUNYEON
N RUPERT
D RUSIN
M ZOLTOSKI
AMSRD ARL WM TB
P BAKER
A GUPTA
AMSRD ARL WM TC
R COATES
T FARRAND
K KIMSEY
L MAGNESS
D SCHEFFLER
R SUMMERS
W WALTERS
AMSRD ARL WM TD
T BJERKE
J CLAYTON
D DANDEKAR
M GREENFIELD
K IYER
J MCCAULEY (20 CPS)
H MEYER
E RAPACKI
M SCHEIDLER
S SCHOENFELD
S SEGLETES
T WEERASOORIYA

NO. OF COPIES	ORGANIZATION
11	FRAUNHOFER-INSTITUT FÜR KURZZEITDYNAMIK (EMI) PROF DR K THOMA DIPL-PHYS E STRAßBURGER (10 CPS) AM KLINGELBERG 1, D - 79588 EFRINGEN-KIRCHEN GERMANY

INTENTIONALLY LEFT BLANK.